Extending the Transient Plane Source Scanning method for determining the specific heat capacity of low thermal conductivity materials through a

Thermochimica Acta 742 (2024) 179883

Contents lists available at ScienceDirect

Thermochimica Acta

journal homepage: www.elsevier.com/locate/tca

Extending the Transient Plane Source Scanning method for determining the specific heat capacity of low thermal conductivity materials through a numerical study

Zijin Zeng [a,b,*], Christian Müller [a], Besira Mihiretie [b]

[a] Department of Chemistry and Chemical Engineering, Chalmers University of Technology, Gothenburg, 41296, Sweden
[b] Hot Disk AB, Sven Hultins gatan 9A, Gothenburg, 41288, Sweden

ARTICLE INFO

Keywords:
Specific heat capacity
Transient plane source scanning method
Finite element method
Polymer
Sensitive analysis

ABSTRACT

In contrast to the conventional Transient Plane Source (TPS) method, the Transient Plane Source Scanning (TPSS) technique allows for the direct determination of the specific heat capacity and requires the use of a specially designed sample holder for accurate measurements. While this method correctly determines the specific heat capacity of samples with moderate and high thermal conductivity, it tends to underestimate the values for those with low thermal conductivity. This paper demonstrates that the underestimated specific heat capacity results from heat loss during the measurement process. To precisely quantify the heat loss, a numerical model based on the finite element method was developed, with key material properties tuned based on measurement data. This model can closely describe the curve of measured thermal response, thereby enabling the precise determination of the specific heat capacity. Consequently, this study introduces a novel approach that incorporates numerical simulation to enhance TPSS measurements of poorly conducting samples, providing a reliable alternative for determining the specific heat capacity.

1. Introduction

The specific heat capacity (C_p) refers to the energy necessary to raise the temperature of a unit mass of material by a finite difference in temperature [1]. It plays a vital role in the design of devices for thermal management. Accurate measurements are essential for optimizing system behavior in industries like aerospace [2,3], automotive [3–5], energy storage [6,7], construction [8–10] etc.

Calorimetry methods such as differential scanning calorimetry (DSC) [11], drop calorimetry [12], adiabatic calorimetry [13,14], and recently the Transient Plane Scanning Source (TPSS) method [15] are commonly used to directly measure C_p.

The Transient Plane Source (TPS) method has been used to characterize a wide range of materials, such as polymers [16,17], building materials [18], textiles [19,20], and graphene composites [21,22]. This method utilizes a thin metal structure in the shape of a double spiral, which performs two simultaneous functions: (1) it serves as a heat source through Joule heating of the spiral and hence the surrounding material, and (2) acts as a sensing element that records a response curve of temperature increase, $\Delta T(t)$, that results from the heating [23]. This response curve is referred to as the temperature transient or thermal response in the text below. Since the resistance of the sensor changes with temperature, the Joule heating alters the electrical resistance of the metal spiral, which disrupts the balance of the Wheatstone bridge. The resulting imbalance in voltage is measured with a sensitive voltmeter. Given the temperature coefficient of resistance, a, and the initial resistance, R_0, of the sensor, one can relate the average temperature change of the sensor to its electrical resistance over time, $R(t)$, as follows [24]:

$$R(t) = R_0[1 + a \cdot \Delta T(t)] \tag{1}$$

In this study, a nickel metal embedded between two protective polyimide (Kapton) films is utilized as the sensor (Fig. 1a), as it offers a well-defined temperature coefficient of resistance. Using this method, it is possible to calculate the thermal conductivity and thermal diffusivity from a single measurement of thermal response curve $\Delta T(t)$ according to Eq. (2) [23].

$$\Delta T(\tau) = P(\pi^{3/2} r \lambda)^{-1} D(\tau) \tag{2}$$

where P is the heating power from the sensor, r is the radius of the sensor, λ is the thermal conductivity of the specimen material, and $D(\tau)$

* Corresponding author at: Department of Chemistry and Chemical Engineering, Chalmers University of Technology, Gothenburg, 41296, Sweden.
E-mail addresses: zijin@chalmers.se (Z. Zeng), besira.mihiretie@hotdiskinstruments.com (B. Mihiretie).

https://doi.org/10.1016/j.tca.2024.179883
Received 12 August 2024; Received in revised form 18 October 2024; Accepted 19 October 2024
Available online 28 October 2024

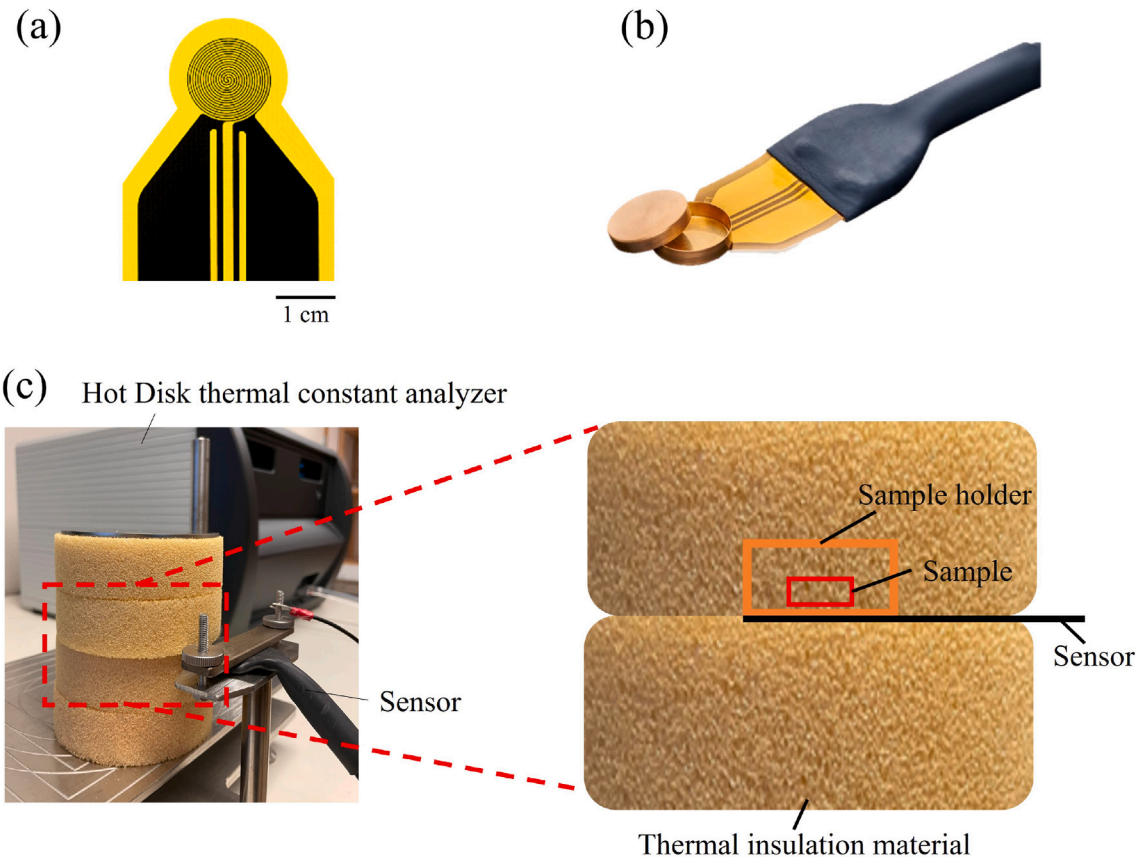

Fig. 1. Sensor profile and schematic of the measurement setup (a) Hot Disk Sensor 5501 insulated by polyimide films. (b) Gold sample holder attached to a Hot Disk Sensor 5501. (c) Schematic of a measurement with a sample.

is a dimensionless time function of τ, which is defined as a function of thermal diffusivity, α and measurement time, t [23].

$$\tau = \left(\frac{t}{\theta}\right)^{1/2} \quad and \quad \theta = r^2/\alpha \tag{3}$$

In instances where both thermal conductivity and thermal diffusivity can be simultaneously determined from an iterative data fitting of the experimentally recorded temperature transient in accordance with Eq. (2), the volumetric heat capacity, ρC_p, of a specimen with density ρ can be calculated using:

$$\rho C_p = \lambda/\alpha \tag{4}$$

Determining the ρC_p from λ and α is applicable to homogeneous isotropic materials like powders, pastes, and pure metals that feature a specific sample size and thermal transport properties [25]. This method offers a reliable and practical approach for determining the specific heat capacity of relatively large specimens. Following this approach, authors in ref [26] measured the C_p of polymers, including poly(methyl methacrylate) (PMMA), across a wide temperature range (from 25 K to 400 K).

Similarly, for a homogeneous slab specimen, the Hot Disk Slab method [27] allows for the simultaneous measurement of the in-plane thermal conductivity and thermal diffusivity using only one temperature transient, leading to the determination of the volumetric specific heat capacity. However, challenges may arise when dealing with small samples with high thermal conductivity even if isotropic, rod-shaped specimens, or extremely conductive slabs are investigated [25].

On the other hand, for materials that are anisotropic and/or inhomogeneous, like many of the contemporary samples produced in the industries mentioned earlier, using Eq. (4) to determine the C_p is not feasible. In fact, it is essential to know the volumetric heat capacity of materials beforehand if one aims to extract the direction-dependent thermal conductivity and thermal diffusivity from temperature transients [28,29]. This necessity motivated the development of the TPSS method, which utilizes the same experimental instrument (the thermal constant analyzer supplied by Hot Disk AB, Gothenburg, Sweden) as the TPS method but with the addition of sample holder and distinct algorithms (see Section 2 for more details). However, the TPSS method presents challenges when measuring materials with a thermal conductivity lower than approximately 1 W/(m K) [30].

It is also possible to employ the Dynamic Plane Source (DPS) approach [31,32] for characterizing the C_p of high-conductivity materials directly. This method is similar to the TPPS method but does not require a special sample holder. To accurately determine C_p with this method, certain criteria must be met. For example, the thermal mass of the sample must be significantly higher than that of the sensor, posing challenges for materials with a low thermal conductivity. Additionally, the thermal conductivity of the sample should be at least 100 times that of its insulating surroundings [25]. For example, using an expanded polystyrene foam (EPS) with a thermal conductivity close to 0.03 W/(m K) sets the approximate working range for the required thermal conductivity to greater than 3 W/(m K).

Numerous experimental and numerical investigations have been conducted to validate the standard TPS method [33–41] , and several sensitivity analyses have been carried out to provide valuable information for thermal properties identification and experimental design [42–44]. However, to the best of our knowledge, studies regarding the TPSS method are rare, and no study has been conducted to improve this method for low thermal conductivity materials.

In summary, the TPSS method is mainly suited for materials with a relatively high thermal conductivity (>1 W/(m K)). This study aims to

extend its applicability to low thermal conductivity materials, including most polymers. To achieve this, a finite element method (FEM) model is developed, which permits to optimize data fitting and analysis, and thus aids in identifying relevant parameters that may contribute to potential sources of error, such as heat loss to the surrounding insulation materials. By understanding these factors, a well-tuned simulation model is proposed that enables accurate data extraction of the C_p. The improvement of the developed model is then evaluated by testing it on a PMMA polymer, which has a low thermal conductivity of approximately 0.19 W/(m K) [45], as well as on glass (approximately 1.0 W/(m K)) and copper samples (approximately 398 W/(m K)).

2. The transient plane source scanning method

This section first introduces the experimental setup, the theoretical framework supporting the TPSS method, and the subsequent data analysis for C_p determination. It is followed by a systematic experimental study on representative samples, illustrating the current capabilities and limitations of the method.

2.1. Experimental setup and theory

As outlined in the previous section, the TPSS method necessitates an additional sample holder and enables the direct measurement of the C_p. In this study, the sample holder is made of a gold alloy with a gold purity of 75% (Fig. 1b).

Two steps are involved in the TPSS method [15]. First, a measurement is conducted with an empty sample holder, referred to as the holder measurement. This step provides crucial information regarding the C_p of the sample holder itself and the heat loss occurring during the measurement. The second step is to conduct a measurement with the sample placed inside the sample holder, referred to as the sample measurement. In both cases, the sample holder is sandwiched between insulation materials (Fig. 1c), which minimizes heat loss.

For the first step, the holder measurement, the specific heat capacity equation can be expressed as follows [15]:

$$P_h = [(mC_p)_h + f_h(t)]\frac{d}{dt}(\Delta T_h(t)) \tag{5}$$

where P_h represents the power input from the sensor during the holder measurement, $(mC_p)_h$ is the heat capacity of the sample holder, and $\frac{d}{dt}(\Delta T_h(t))$ represents the rate of temperature increase of the sensor. It is assumed that there exists a heat loss equation [15], denoted as $f(t)$, which governs the rate of heat loss during the measurement by $Q(t) = \frac{d}{dt}(\Delta T(t))f(t)$. $f_h(t)$ is the heat loss equation for the holder measurement.

During the second step, the sample measurement, we assume that the sensor adequately captures the thermal response of the sample after a certain time [15,25]. The total measurement time should be long compared to this certain time duration. A detailed discussion about how to decide the total measurement time can be found in Section 2.2. Based on these assumptions, Eq. (6) can be written for the sample measurement in a similar manner as Eq. (5) [15]:

$$P_s = [(mC_p)_h + (mC_p)_s + f_s(t)]\frac{d}{dt}(\Delta T_s(t)) \tag{6}$$

where P_s represents the power input from the sensor during the sample measurement, $(mC_p)_s$ is the heat capacity of the sample, $\frac{d}{dt}(\Delta T_s(t))$ represents the rate of temperature increase of the sensor during the sample measurement, and $f_s(t)$ is the heat loss equation for the sample measurement. The heating power during the sample measurement should be increased to achieve a similar temperature increase as observed for the holder measurement [30]. In the phase of the measurement where the $\Delta T_h(t)$ and $\Delta T_s(t)$ exhibit linear alignment, it is assumed that $f_h(t)$ is equivalent to $f_s(t)$. This assumption allows for the derivation of a final equation to calculate the heat capacity of the sample [15]:

$$\frac{\overline{P_s}}{\delta_s} - \frac{\overline{P_h}}{\delta_h} = (mC_p)_s \tag{7}$$

where $\overline{P}$ is the average power input from the sensor and δ is the average rate of temperature increase, defined as $\frac{d}{dt}\overline{\Delta T(t)}$.

Table 1
Three types of samples and the expected time ranges for calculating C_p.

Material	Expected time ranges
Copper	20–40 s
Glass	40–80 s
PMMA	120–240 s

2.2. The determination of total measurement time

In both case of the holder measurement and sample measurement, the measurement time should be longer than the time it takes to establish a non-varying temperature gradient inside the holder or holder-sample assembly. After the non-varying temperature gradient is established, the recorded $\frac{d}{dt}(\Delta T(t))$ of the sensor can represent that of the sample holder or holder-sample assembly, which is the foundation of Eq. (5) and Eq. (6).

In an ideal case, where a cylindrical sample is heated by a uniform and constant heat flux from its bottom surface (see inset of Fig. 2a), and assuming no heat loss, the time needed to establish a non-varying temperature gradient within the sample, known as the settling time, can be estimated by ${l_s}^2/\alpha$. Here, α denotes thermal diffusivity, l represents the characteristic length [15,25], and subscript s refers to the sample. The characteristic length of the sample is its height in the direction perpendicular to the sensor surface.

On the other hand, for a measurement where an additional sample holder is utilized (this work), the settling time could be estimated using $(\frac{l_s}{\sqrt{\alpha_s}} + \frac{l_h}{\sqrt{\alpha_h}})^2$, where subscript h denotes the sample holder [15,25]. In actual cases where the sample holder has a much higher thermal diffusivity than the sample, $2\,{l_s}^2/\alpha$ is utilized for calculating the settling time of the holder-sample assembly [25,30]. In addition, it is recommended that data analysis should focus on the time range between $2 \cdot l_s^2/\alpha$ to $4 \cdot l_s^2/\alpha$ seconds for the subsequent heat capacity calculation [25,30]. The time ranges based on this recommendation were utilized in the following section for C_p calculation.

2.3. Experimental results and data analysis

Utilizing the aforementioned two-step experimental procedure, the precise determination of the power delivered to the sample, which is instrumental in influencing the temperature throughout the entire bulk specimen, can be achieved. Furthermore, the average rate of temperature rise, δ, is calculated from the measured data within a recommended time range. This allows for the determination of the C_p using Eq. (7). Data from different time ranges were used to calculate the specific heat capacity of different samples. Table 1 provides an overview of the sample types and expected time ranges. The reason and the detailed methodology for deciding the time ranges are explained in Section 2.2. As outlined, the selection of the time range depends on the thickness and thermal diffusivity of the sample. It should be noted that the settling time of the gold sample holder must also be considered, which is circa 20 s; hence the earliest time range should start from 20 s.

To systematically evaluate the existing measurement method, we measured the temperature transient of samples with varying thermal diffusivity at room temperature (293 K). Exemplary temperature transients of the holder measurement and sample measurement of different samples are shown in Fig. 2b. Heating powers used during the measurements were as follows: 80 mW for the holder measurement, 160 mW for copper, and 130 mW for both copper and PMMA. These sample types consisted of 99% pure copper, float glass obtained from VWR, and atactic PMMA with a weight-average molecular weight (Mw) of 94 kg/mol and a polydispersity index (PDI) of 1.5, sourced from Polysciences. The thermal conductivity of PMMA at room temperature is expected to be approximately 0.19 W/(m K) [45].

The comparison of C_p of those samples is presented in Fig. 2c. The reference C_p of the glass and PMMA in Fig. 2c are determined using

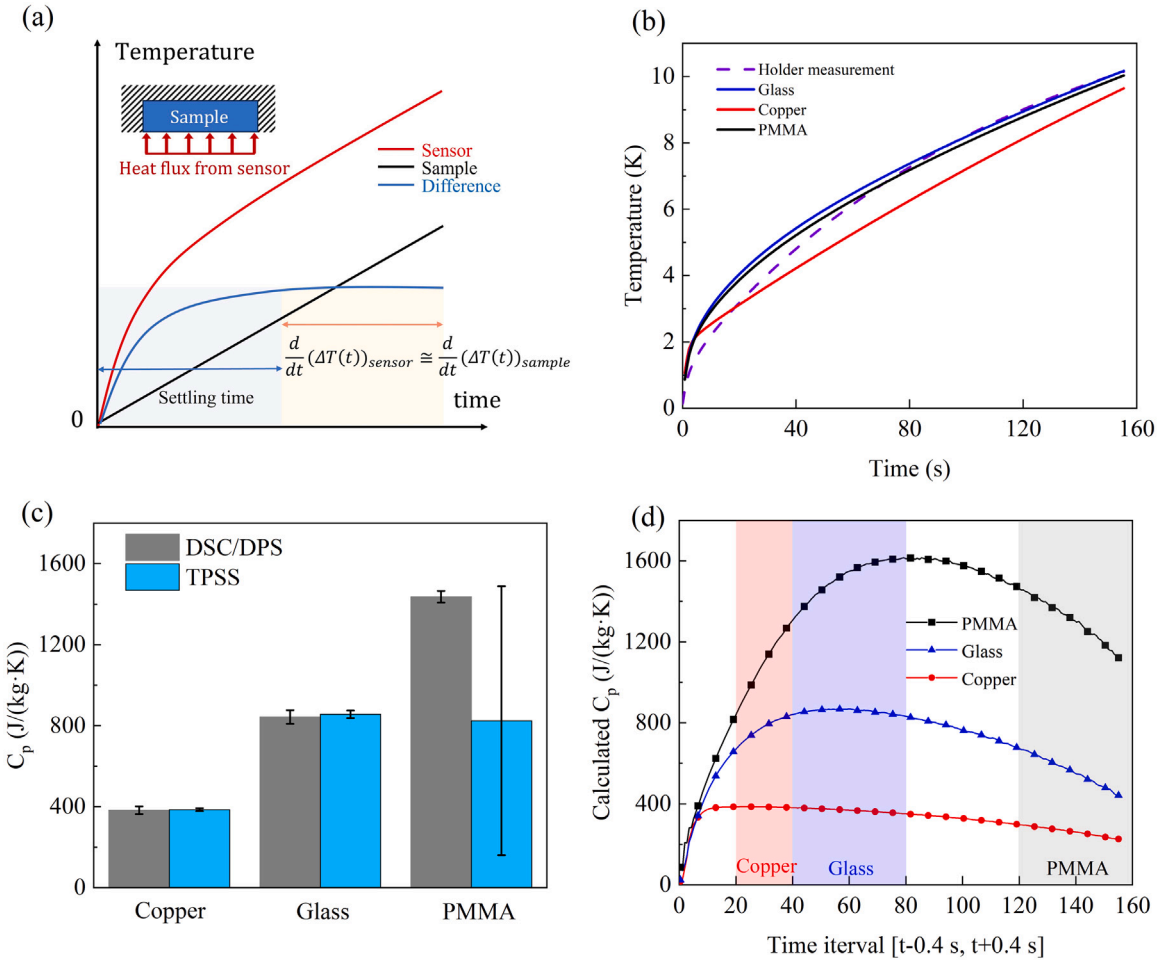

Fig. 2. (a) Comparison of average temperature increase between the sensor and sample in an ideal scenario, where a cylindrical sample is heated by a uniform heat flux from its bottom, with no heat loss (see inset). (b) Temperature transient (temperature increase over time) measured by the sensor in the holder measurement and the sample measurements. (c) Comparison between C_p of the samples at room temperature (293 K) obtained from the TPSS method and reference values from DSC[1](glass, PMMA) or DPS[2](copper). (d) The value of C_p calculated using moving time windows ([t-0.4 s, t+0.4 s]) with a short interval of 0.8 s.

DSC. Instead, the reference specific heat capacity of copper is obtained using the DPS method [32], which is reliable for samples with a high thermal conductivity. Each reported TPSS value of average C_p is based on three measurements. The error bars are related to the fluctuation of calculated C_p within corresponding time ranges (Fig. 2d).

The average TPSS values for copper and glass are in good agreement with the reference values, but the value for PMMA is significantly underestimated. To preliminarily investigate the cause of the underestimation, we recalculated the C_p using moving time windows [t-0.4 s, t+0.4 s] with a small interval of 0.8 s [41], instead of all the data from the expected time range. Here, t represents the central point of the time window. In our measurements, an interval of 0.8 s is used to record data across all three types of samples, serving as the thermal response sensing period. Consequently, this 0.8 s interval represents the smallest time window available for the determination of C_p. This analysis provides a more detailed insight into how the calculated values of C_p evolve over time.

It is observed that the calculated C_p of all the samples initially increases and then declines over time (Fig. 2d). The colored regions indicate the time ranges for calculating C_p of copper and glass. In the case of the copper sample, the increasing phase is notably shorter than that of the other samples, owing to its high thermal diffusivity. Within 20 s to 40 s, there is a range of data with a minimal fluctuation of around 1%. For the glass sample, the fluctuation of C_p from 40 s to 80 s is noticeably larger, around 3%. For copper and glass, a state could be reached where the heat loss has a relatively small impact on the measurement accuracy. However, when the data outside this state is used to calculate the C_p, the results are inaccurate. This implies that the measurement results are sensitive to the selection of the time window utilized for the calculation.

In contrast, for the PMMA sample, there is a 13% drop in C_p from 120 s to 160 s. If the data is extrapolated linearly to 240 s, the drop from 120 s to 240 s is expected to be even more significant. Since the calculated C_p of PMMA around 160 s is already much lower than the reference value and is expected to decrease further over time, the data from 160 s to 240 s were not experimentally obtained but extrapolated by a linear fit.

3. Numerical simulation

In this section, we present a simulation model using finite element method (FEM) (Section 3.1) and proceed to describe a modeling approach we term ‘a well-tuned model’, grounded in TPSS measurement data (Section 3.2).

[1] Measured using a DSC 2 calorimeter supplied by Mettler Toledo, Greifensee, Switzerland.

[2] Measured using a thermal constant analyzer supplied by Hot Disk AB, Gothenburg, Sweden.

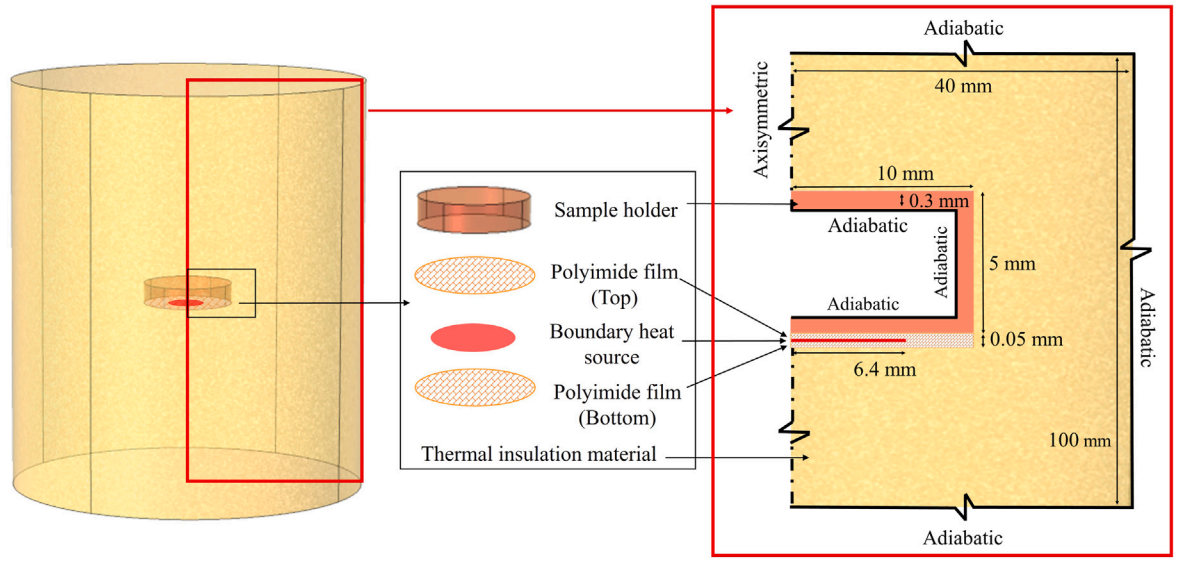

Fig. 3. Schematic of the model accompanied by its cross-sectional view. Selected components have been scaled in the cross-sectional view to accommodate the wide range of dimensions and ensure all elements are discernible. An ideal heat source with a circular boundary (marked in red) is used to represent the double spiral sensing element.

3.1. The development of a FEM model

A 3-dimensional (3D) FEM simulation of the TPSS experimental approach was reported in Ref. [46]. These simulation results demonstrated good agreement with high and moderately conducting materials. However, it was noted that for low thermal conductivity materials, the TPSS method tends to underestimate the C_p values, an issue this study aims to address. Due to the nearly axisymmetric nature of the measurement setup, its simulation model can be simplified to two dimensions (2D) [37,40]. For the current study, which involves the analysis of multiple parameters, a 2D simulation was chosen. This preference is due to its efficiency in accurately capturing heat transfer properties while also reducing the computational time. Furthermore, a mesh independence analysis was conducted to select the optimum mesh configuration for accuracy and computational efficiency (Fig. S1).

A detailed visualization of each component within the model is achieved through a 3D representation, crafted by rotating the 2D geometry, and is accompanied by dimensional details (Fig. 3) that correspond to the experimental TPSS counterpart.

To simplify the simulation model, the following assumption were made:

- The heat transfer between measurement setup and ambient environment is negligible (adiabatic boundary condition).
- Inside the setup, heat transfer via convection and radiation is negligible.
- The measurement setup is axisymmetric, which means the effect from sensor leads, and the non-circular shape of the sample, are negligible.
- Material properties are assumed to be constant during the measurement.
- The spiral sensing element of the sensor can be represented by an ideal circle boundary heat source.

Material properties utilized in these simulations are summarized in Table 2. The simulation utilized the heat transfer module for solids in COMSOL Multiphysics, and the governing equations for non-steady state heat conduction employed in the simulation are presented as follows:

$$\rho C_p \frac{\partial T}{\partial t} + \nabla q = \phi \tag{8}$$

$$q = -\lambda \nabla T \tag{9}$$

Table 2
Summary of the component properties used in the simulation for sensitivity analysis.

Component	Material	λ (W/(m K))	C_p (J/(kg K))	ρ (kg/m^3)
Sample holder	Gold alloy	44 ± 10[a]	177[b]	15500[c]
Insulation material	Polyimide foam	0.039 ± 0.002[d]	1090[e]	6.6[c]
Polyimide film	Polyimide	0.12[e]	1090[e]	1420[e]

[a] Measured by the Hot Disk slab method [27].
[b] Calculated based on the specific heat capacity of the ingredients.
[c] Calculated from mass and volume.
[d] Measured by the Hot Disk isotropic method [24].
[e] Obtained from Ref. [47].

where q denotes heat flux by conduction, while ϕ is the power supplied from the heat source. The thermal contact resistance, R_c, is integrated in the simulation model by assigning an equivalent thin resistive layer between the geometry of the sample and sample holder. The heat conduction across the resistive layer is governed by,

$$q = \frac{1}{R_c}(T_h - T_s) \tag{10}$$

where T_h and T_s are the temperature sample holder and the sample at their contact interface, respectively.

3.2. Development of the well-tuned model

The development and utilization of the well-tuned model consists of four steps (Fig. 4).

Firstly, a FEM model (Section 3.1) based on the actual experimental setup and the components used in the holder measurement (without sample) was developed.

Secondly, we employed the FEM model to conduct a sensitivity analysis to different material properties. According to the sensitivity analysis, we identify four crucial parameters that potentially influence the thermal response in the holder measurement to a significant degree.

Thirdly, these identified key parameters were finely tuned through a parameter estimation analysis that utilized data from the holder measurement, resulting in the well-tuned model which can closely describe the actual measurement.

In a final step, a sample was added to the well-tuned model, while the four key parameters obtained in the previous step were held constant. Sample measurement data were then incorporated into the model

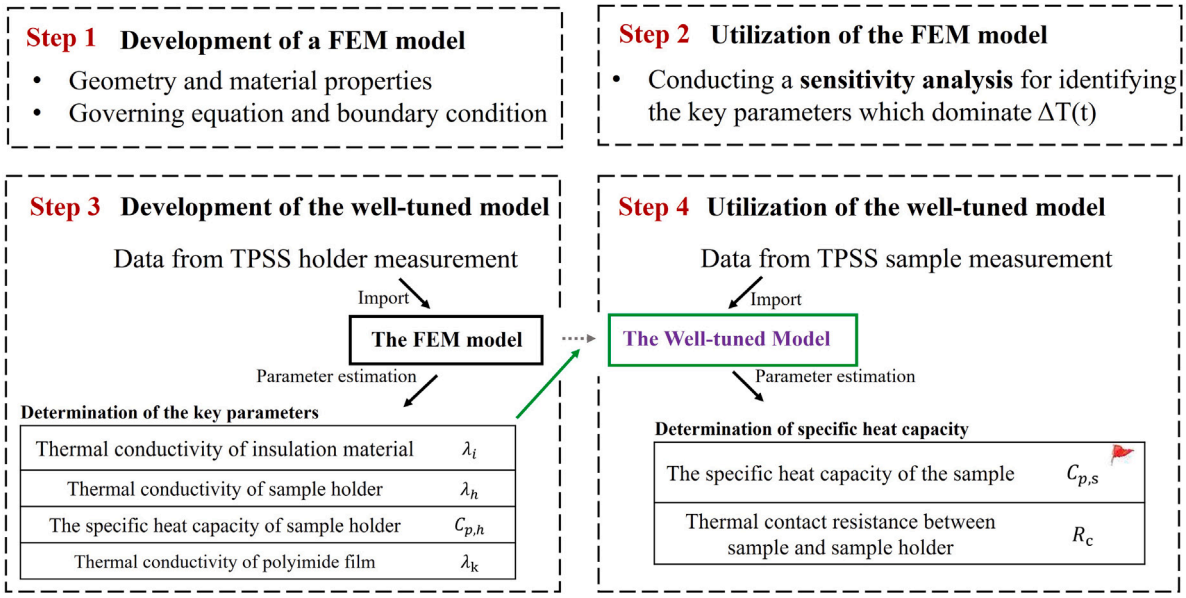

Fig. 4. The work flow of the simulation, including the development of the well-tuned model and its implementation.

for another parameter estimation analysis, enabling the determination of the C_p of the sample.

3.2.1. Sensitivity analysis

In the sensitivity study, a simulation based on the parameters in Table 2 was conducted to find out how a change in parameter x influences $\Delta T(t)$ in the measurement, namely the sensitivity coefficient $S_x(t)$. Following Ref. [42,48,49], we define $S_x(t)$ as the difference of thermal response caused by changing a parameter x by a certain tolerance of ϵ. To determine $S_x(t)$, a parameter sweep study is conducted with the target parameter being assigned to different values ($\epsilon = 0.1\%$), while keeping other parameters fixed. Using the equation below, $S_x(t)$ is calculated from the thermal response,

$$S_x(t) = \frac{\Delta T_{x+\epsilon}(t) - \Delta T_x(t)}{\epsilon} \tag{11}$$

The outcomes of $S_x(t)$ distinctly demonstrate that different parameters have specific impacts on $\Delta T(t)$, as illustrated in Fig. 5a and Fig. 5b. In the holder measurement, the sample holder plays a crucial role in the holder measurement, with its thermal conductivity (λ_h) and specific heat capacity ($C_{p,h}$) considerably affecting $\Delta T(t)$. The thermal conductivity of the insulation material (λ_i) also markedly influences $\Delta T(t)$ and its influence increases dramatically with time. Additionally, the thermal conductivity of the polyimide film (λ_k) is another parameter of interest. Since an ideal circular boundary heat source was employed to represent the spiral sensing element, λ_k in the simulation serves as an equivalent thermal conductivity that enables the ideal heat source to accurately replicate the behavior of the actual spiral. Therefore, these four parameters are selected to be tuned based on the data from the holder measurement.

In the parameter estimation, it is necessary to determine if the parameters being estimated exhibit linear correlation within the input data range. If such correlation exists, simultaneous estimation of the correlated parameters becomes infeasible [48]. During the period after 20 s, the sensitivity to λ_k (S_{λ_k}) and λ_h (S_{λ_h}) tends to remain constant. This implies that these two parameters are not correlated with the other two parameters, λ_i and $C_{p,h}$, whose sensitivity (S_{λ_i}, $S_{C_{p,h}}$) varies over time with different derivatives. S_{λ_i} has no linear correlation with $S_{C_{p,h}}$ throughout 160 s, while S_{λ_k} tends to be linearly correlated with S_{λ_h} after 20 s (Fig. S2a). The non-linear relationship between S_{λ_k} and S_{λ_h} from 10 s to 20 s still allows for the simultaneous estimation of these two parameters based on the measured data.

A sensitivity analysis was conducted for a measurement of copper (Fig. 5b). In this case, the sensitivity to the specific heat of the copper ($S_{C_{p,c}}$) increases over time, which is in agreement with other transient measurements of C_p in a thermal-insulated condition [50,51]. The sensitivity of the equivalent thermal contact resistance between the sample and the sample holder (S_{R_c}) remains constant at an appreciable level after a short period and does not correlate with $S_{C_{p,c}}$. Therefore, these two parameters could be estimated at the same time.

On the other hand, the sensitivity to λ_i (S_{λ_i}) and $C_{p,h}$ ($S_{C_{p,h}}$) rises over time. These two parameters were estimated in step 3 and utilized as the input parameters when estimating $C_{p,c}$. Relatively high sensitivity to these parameters suggests that their uncertainty has a greater influence on the final result of $C_{p,c}$. When considering the influence of λ_i, time windows starting after 20 s are preferred because of a higher relative sensitivity to the specific heat capacity of copper ($S_{C_{p,c}}/S_{\lambda_i}$, Fig. S2b). Meanwhile, $S_{C_{p,c}}/S_{C_{p,h}}$ remains relatively constant after 20 s, indicating the data after this time are comparable in terms of the potential influence of $C_{p,h}$.

Overall, λ_h, $C_{p,h}$, λ_i, and λ_k could be simultaneously identified in step 3, while the specific heat capacity of the sample ($C_{p,s}$) and R_c could be estimated in step 4.

3.2.2. Parameter estimation and model validation

The well-tuned model shares the same physical framework as the FEM model developed in the previous section. However, the four key material properties (λ_h, $C_{p,h}$, λ_i, λ_k) in the well-tuned model were determined through a parameter estimation study (step 3) based on the holder measurement data. Specifically, the data from 10 s to 160 s, with a heating power of 80 mW, were utilized. In step 4, the time windows immediately after the sample achieved a non-varying temperature gradient were utilized: 20 s to 40 s for copper, 40 s to 80 s for glass, and 120 s to 160 s for PMMA.

The parameter estimation study is based on the least-square method governed by the following equation,

$$J = \sum_{n=t}^{t+\Delta t} [\Delta \tilde{T}_n(\lambda_h, C_{p,h}, \lambda_i, \lambda_k) - \Delta T_n]^2/2 \tag{12}$$

where J is the least-square objective value, $\Delta \tilde{T}_n$ represents the simulated average temperature increase of the sensor and ΔT_n corresponds to the measured average temperature increase, both evaluated at various time points t.

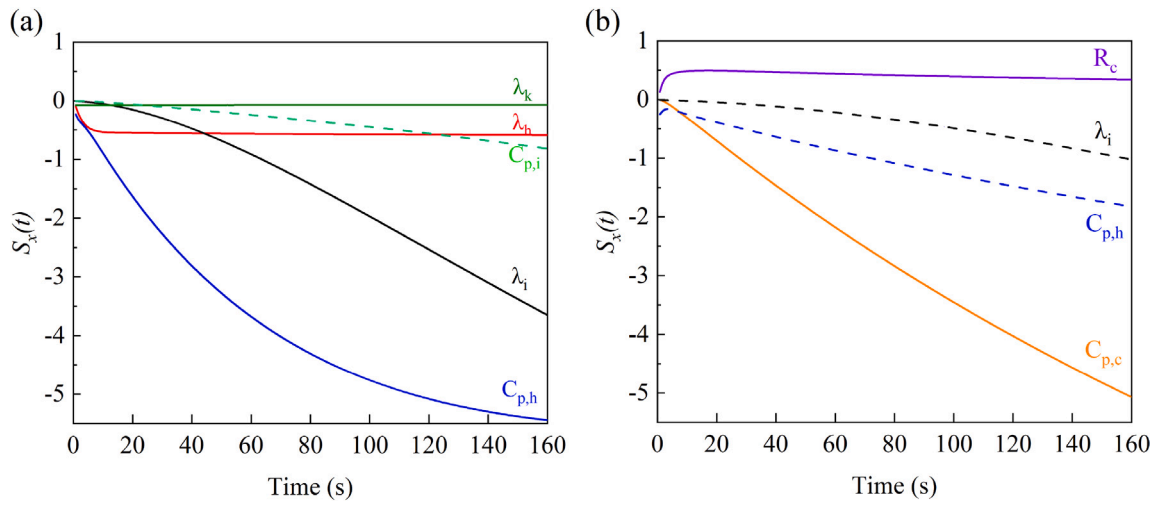

Fig. 5. (a) The sensitivity coefficient $S_x(t)$ for $C_{p,h}$, λ_i, λ_h, $C_{p,i}$ and λ_k obtained from the FEM model of the holder measurement. The sensitivity to the parameters estimated in step 3 are represented by solid lines. (b) $S_x(t)$ for $C_{p,c}$, $C_{p,h}$, R_c, and λ_i obtained from the FEM model of copper measurement. The sensitivity to the parameters estimated in step 4 are represented by solid lines.

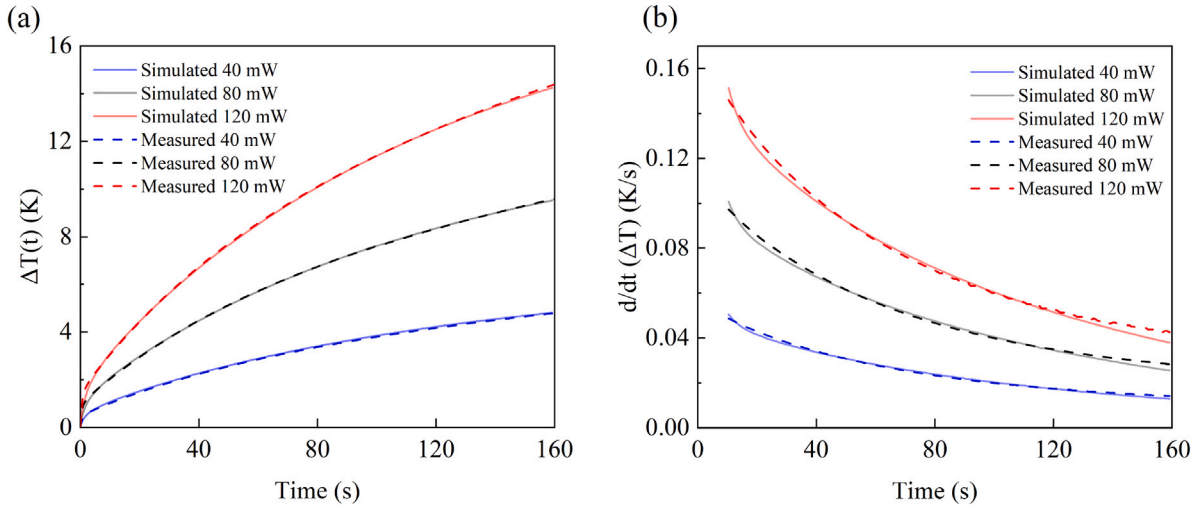

Fig. 6. (a) Comparison of the average $\Delta T(t)$ of the sensor between the measurements (dashed lines) and the well-tuned model (solid lines) for a heating power of 40 mW (blue), 80 mW (black), and 120 mW (red). (b) Comparison of the first derivative of $\Delta T(t)$ between the measurement and the well-tuned model.

Table 3
Average effective values from three trials of parameter estimation, each based on different sets of hold measurement data.

Parameter	Estimated value
λ_h (W/(m K))	34.6 ± 1.1
λ_i (W/(m K))	0.057 ± 0.001
λ_k (W/(m K))	0.017 ± 0.002
$C_{p,h}$ (J/(kg K))	153.5 ± 4.3

In the parameter estimation, a derivative-free optimization method, specifically the bound optimization by quadratic approximation (BOBYQA), has been employed. The core principle of the BOBYQA method involves iteratively approximating the objective function with a suitable quadratic model [52].

To validate the model resulting from this step, we initially compared the measured and simulated $\Delta T(t)$ for different power values (Fig. 6a). Note that only the measured data with a heating power of 80 mW was utilized in step 3. The maximum difference observed between the simulated and measured data was 1%, indicating that the model from step 3 accurately describes and predicts the thermal response. Furthermore, the derivatives of $\Delta T(t)$ from both the measurement and the simulation were compared (Fig. 6b), showing a good correlation between the two.

4. Results and discussion

4.1. Determination of $C_{p,s}$

The $\Delta T(t)$ obtained from the holder measurement was used to extract the four effective parameters: λ_h, $C_{p,h}$, λ_i, and λ_k (Table 3). However, the actual measurement setup is more intricate than this simulation model which is based on several assumptions (Section 3.1). For example, the actual sensing element (nickel spiral) is represented by an ideal boundary heat source. In addition, the sensor comprises two polyimide layers on opposite sides of the nickel wire with an adhesive layer in between. As a result, the estimated parameters are termed "effective values", whose sole purpose is to serve as calibration/fitting parameters for the next step of the simulation.

The parameters derived during step 3 were subsequently used in step 4 to determinate the specific heat capacity of the sample ($C_{p,s}$). The average $C_{p,s}$ of each sample in Table 4 were obtained from nine trials.

Table 4
The comparison between the reference value and the C_p of samples determined by the parameter estimation (step 4). The estimated values are based on nine trials for three samples (three trials for each sample).

C_p (J/(kg K))	Trial	Copper	Glass	PMMA
Sample A	1	381.8	836.1	1393.2
	2	385.8	837.4	1426.6
	3	381.4	836.0	1382.4
Sample B	4	377.5	781.3	1477.2
	5	379.7	777.3	1473.3
	6	380.8	782.7	1490.9
Sample C	7	379.2	801.8	1401.9
	8	383.2	806.1	1401.8
	9	379.4	801.7	1402.5
Average		381.0 ± 19.1	806.7 ± 40.3	1427.8 ± 71.4
Reference		384.2 ± 19.2[a]	843.3 ± 34.0[b]	1436.7 ± 28.7[b]

[a] Measured by DPS.
[b] Measured by DSC.

The average values are close to corresponding reference values, with an average difference of less than 4.4%. This demonstrates the ability of the model to accurately determine the $C_{p,s}$ based on experimental data.

However, it was anticipated that the results of $C_{p,s}$ were influenced by the uncertainty of input parameters, including the specific heat capacity of the insulation material ($C_{p,i}$), the thermal conductivity of the sample (λ_s), and the selection of the time window. The influence of these factors on the final result of $C_{p,s}$ can be investigated by varying these factors, respectively [33,53]. The results in Fig. S3 show that the estimated $C_{p,s}$ is weakly sensitive to the changes in $C_{p,i}$ and λ_s, and time window. Furthermore, considering that the uncertainties resulting from these factors are independent and small, Eq. (13) was employed to estimate the total uncertainty (U) in the parameter estimation process [50,53,54],

$$U = \sqrt{{U_{\Delta tw}}^2 + {U_{\Delta C_{p,i}}}^2 + {U_{\Delta \lambda_s}}^2} \tag{13}$$

where $U_{\Delta tw}$, $U_{\Delta C_{p,i}}$, and $U_{\Delta \lambda_s}$ are the fractional changes in the results of $C_{p,s}$ due to changes in the time window, $C_{p,i}$, and λ_s, respectively. The final uncertainty in parameter estimation was calculated to be 0.7%, 1.1% and 6.7% for copper, glass, and PMMA, given a 30% uncertainty in the three factors. When a reliable value of $C_{p,i}$ (uncertainty less than 10%) is used as an input parameter, the final uncertainty are 0.3%, 0.4%, and 4.3%, even with a 30% uncertainty in the other two factors.

Using the same method, the specific heat capacity of two other polymers at room temperature (293 K), namely high density polyethylene (HDPE) and poly(3-hexylthiophene) (P3HT), were determined to be 1942 ± 97 J/(kg K) and 1608 ± 80 J/(kg K), respectively. HDPE and P3HT were sourced from Sigma-Aldrich and Ossila, respectively. More detailed information including Mw and PDI are provided in Table S1.

4.2. Comparison of $\Delta T(t)$ between sample and the sensor

The calculation of $C_{p,s}$ in TPSS relies on a fundamental assumption: namely that the sensor can precisely capture the rate of average temperature change over time, $\frac{d}{dt}(\Delta T(t))$, for the entire sample. However, in real-world measurements, this assumption may not hold due to factors such as the presence of a sample holder and imperfect thermal insulation materials. In such cases, comparing the differences in $\Delta T(t)$ and $\frac{d}{dt}(\Delta T(t))$ between the sensor and the sample can provide valuable insights into potential errors.

For instance, in the case of copper, its average $\Delta T(t)$ shows a constant offset of around 2 K compared to that of the sensor after a few seconds (as shown in Fig. 7a). The 2 K difference in $\Delta T(t)$ emerges primarily from the thermal resistance between the sensor and the sample, alongside the internal thermal resistance of the sample itself.

In addition, $\frac{d}{dt}(\Delta T(t))$ of the sensor and the copper is compared (Fig. 7c). The difference between these two rates reduces to approximately 2% after a brief duration. This brief duration is estimated to be around 10 s. This duration can not only be attributed to the sensor (sample holder) inertia and thermal contact resistance, but also to the time needed to achieve a non-varying temperature gradient inside the sample. Note that in the TPSS measurement, this brief duration differs from that in the TPS measurement, which accounts for sensor thermal inertia and thermal contact resistance [42–44], but does not require consideration of the non-varying temperature gradient of the sample.

By contrast, the difference in $\Delta T(t)$ between PMMA and the sensor requires more time to reach its peak of around 4 K, and subsequently exhibits a noticeable decline over time (Fig. 7b). These characteristics are attributed to the low thermal diffusivity of PMMA. Likewise, we calculated the difference in $\frac{d}{dt}(\Delta T(t))$ between the PMMA sample and the sensor (Fig. 7d). Notably, this difference increases significantly during the first 100 s and then remains at around 11%. The larger difference in $\frac{d}{dt}(\Delta T(t))$ implies that, in the case of PMMA, heat is more difficult to conduct away from the sensor. This is due to both the thermal contact resistance and the low thermal conductivity of the sample.

4.3. Heat loss in the measurements

The thermal response curve $\Delta T(t)$ is influenced by multiple factors, including the heat capacity of both the sample and the sample holder, heat conduction between the sensor and the sample (thermal contact resistance and the thermal conductivity of the sample), and heat loss to the insulation material. Heat conduction between the sensor and the sample predominantly affects the initial stages of the measurement (for $t < 2 \cdot l_s^2/\alpha$), whereas heat loss becomes more significant over longer timescales.

In this section, the assumption regarding the heat loss equation is examined, namely $f_h(t) = f_s(t)$ (Section 2.1). This assumption holds when $\Delta T(t)$ in both measurements exhibits approximately linear behavior and they are aligned with each other [15]. However, in our measurements, we observe that $\Delta T(t)$ slightly deviates from linearity (Fig. 2b). This deviation arises from the heat loss to the insulation material, and it introduces a potential error in the determination of $C_{p,s}$ from Eq. (7). To gain deeper insight and to quantify the extent of heat loss, we conducted a comprehensive analysis of the heat balance utilizing the well-tuned model.

In the case of the holder measurement (Fig. 8a), the rate of heat accumulation in the sample holder decreases over time. Conversely, the rate of heat accumulation in the insulation material, or in other words, heat loss ($Q(t)$), steadily increases over time and eventually surpasses that of the sample holder at around the 60 s. Ultimately, it becomes three times greater than the heat accumulation in the sample holder, accounting for a substantial 74% of the overall heating power. A large heat loss is undesirable, as it implies that the actual experiment may deviate from ideal conditions.

In the case of the copper measurement (Fig. 8b), a similar trend of $\Delta T(t)$ can be observed for the sample holder and the insulation material. Additionally, a substantial fraction of the heat is directed to the copper sample, resulting in a smaller portion of heat entering the insulation material when compared to the holder measurement. This is the reason why the change in $\Delta T(t)$ during the sample measurement appears to follow a more linear trend compared to that during the holder measurement.

Knowing $Q(t)$ (Fig. 8a–b), we can calculate the unique heat loss function described in Section 2.1 as follows: $f(t) = Q(t)/\frac{d}{dt}(\Delta T(t))$. In the case of the copper sample, the difference between $f_h(t)$ and $f_s(t)$ remains small within the time window of 20 s to 40 s, varying within a range of ±8% (Fig. 8c). However, the difference gradually increases

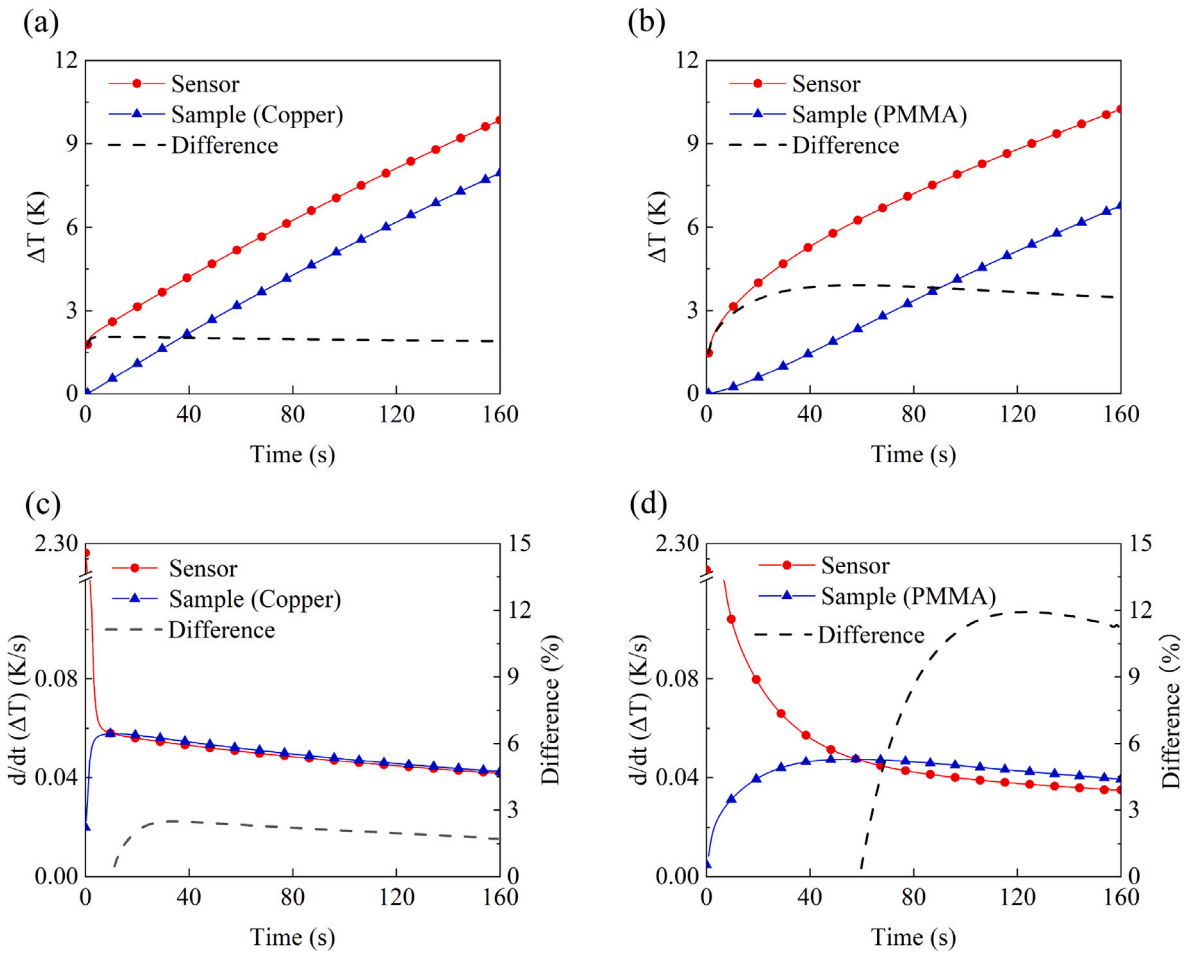

Fig. 7. Average $\Delta T(t)$ of the sensor and the sample for (a) copper and (b) PMMA. The corresponding $\frac{d}{dt}(\Delta T(t))$ for (c) copper and (d) PMMA. The dashed line in each plot represents the difference between the sensor and the sample.

over time and reaches 48% at the end of the measurement, in line with the observed trend of increasing underestimation of $C_{p,s}$ with time (Fig. 2b). For the PMMA sample, $f_h(t) \neq f_s(t)$ throughout the measurement. Initially, $f_h(t)$ is smaller than $f_s(t)$, but surpasses $f_s(t)$ after 100 s and ultimately becomes approximately 20% larger by the end of the measurement.

Furthermore, we estimated the percentage of error in the heat loss calculation relative to the heating power, referred to as $\varepsilon_Q(t)$ (Fig. 8d), using the formula below:

$$\varepsilon_Q(t) = \frac{f_h(t)\frac{d}{dt}(T_s(t)) - Q_s(t)}{P_s} \tag{14}$$

where $Q_s(t)$ represents the rate of heat loss in the sample measurement. For copper, $\varepsilon_Q(t)$ changes from −1% to 16% between 20 s and 160 s. Interestingly, $\varepsilon_Q(t)$ remains within ±1% during the time window of 20 s to 40 s (Fig. 8d, red region). This small value of $\varepsilon_Q(t)$ and the ability of the sensor to accurately capture the $\Delta T(t)$ of copper (Fig. 7a, c) are the reasons why $C_{p,c}$ calculated from this particular time window agrees with the reference value (Fig. 2c). For PMMA, $\varepsilon_Q(t)$ ranges from 3% to 10% within the time window of 120 s to 160 s. A higher $\varepsilon_Q(t)$ implies that the heat loss here is overestimated, which contributes to the underestimation of the specific heat capacity of PMMA ($C_{p,p}$).

In this section, we have quantified $Q(t)$ in both holder and sample measurements, relying on the results from the well-tuned model. It is evident that $Q(t)$ gradually increases over time, eventually accounting for a non-negligible portion of the total heat power. Subsequently, we have demonstrated that the difference between the heat loss equations $f_h(t)$ and $f_s(t)$ is indeed evident, especially in the later part of the measurements. This difference is believed to be the primary source of error in our experimental determination of $C_{p,s}$ for materials with a low thermal conductivity.

5. Conclusions

The objective of this study was to enhance the TPSS method to measure the specific heat capacity of materials with a low thermal conductivity. While the existing method is effective for determining the specific heat capacity of samples with moderate to high thermal conductivity ($\lambda > 1$ W/(m K)), the improved approach extends its applicability to materials with thermal conductivity as low as 0.19 W/(m K).

First, we conducted a series of TPSS experiments of select samples (copper, glass, and PMMA) with varying thermal conductivity to evaluate the measurement method. This analysis revealed both the capabilities and limitations of the TPSS method, particularly its tendency to underestimate the specific heat of samples with a low thermal conductivity. Following this, a well-tuned simulation model was developed and validated using the experiment data, with key material properties determined through a parameter estimation analysis. The simulation model was subsequently utilized to estimate the specific heat capacity of the samples. The estimated specific heat values showed good agreement with reference data, exhibiting a deviation of 4.4% and a small uncertainty. This alignment was achieved by analyzing data from a specific time range, which was determined based on the thickness and thermal diffusivity of each sample. For unknown samples, selecting an appropriate time range would be essential to ensure optimal results.

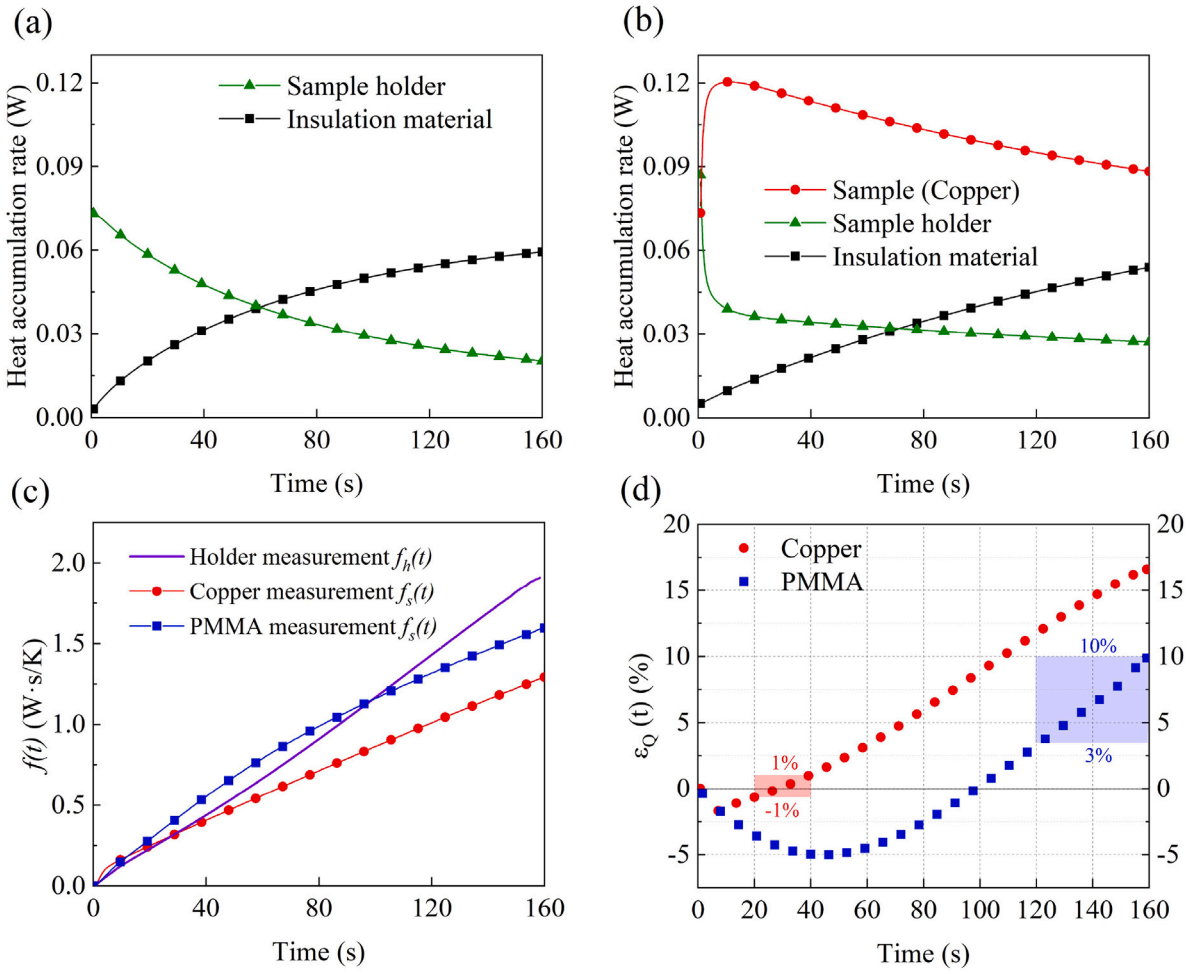

Fig. 8. The rate of heat accumulated in different components during (a) the holder measurement and (b) the sample measurement. (c) Comparison of the unique heat loss function that describes the holder measurement $f_h(t)$ and sample measurement $f_s(t)$. (d) The percentage of error in the heat loss calculation relative to the heating power, defined as $\varepsilon_Q(t)$.

Furthermore, the study illustrates that heat loss during the holder measurement and during the sample measurement could vary significantly, especially during longer measurement times, which is not anticipated in the conventional theory. This variation became evident through a heat balance analysis for each component (sample, sample holder, and thermal insulation material). The analysis led to the conclusion that inaccuracies in heat loss calculations are the primary reason for the underestimation of the specific heat capacity.

In summary, this work enhances the capabilities of the TPSS method by incorporating a well-tuned simulation model, offering a reliable alternative for determining the specific heat capacity of materials with low thermal conductivity.

CRediT authorship contribution statement

Zijin Zeng: Writing – review & editing, Writing – original draft, Visualization, Methodology, Investigation, Formal analysis, Data curation. **Christian Müller:** Writing – review & editing, Supervision, Resources, Project administration, Funding acquisition, Conceptualization. **Besira Mihiretie:** Writing – review & editing, Supervision, Resources, Project administration, Funding acquisition, Conceptualization.

Declaration of competing interest

The authors declare the following financial interests/personal relationships which may be considered as potential competing interests: Zijin Zeng and Besira Mihiretie are affiliates of Hot Disk AB and have a financial interest in the commercial success of the Hot Disk instrument. However, all scientific data and analyses presented in this paper are intended to meet standard scientific criteria for rigor and reproducibility. If there are other authors, they declare that they have no known competing financial interests or personal relationships that could have appeared to influence the work reported in this paper.

Acknowledgments

This project has received funding from the European Union's Horizon 2020 research and innovation program under the Marie Skłodowska-Curie grant agreement No 955837. The authors also wish to thank Dr. Silas Gustafsson for insightful discussion, and Dr. Henrik Otterberg for his thorough language review.

Appendix A. Supplementary data

Supplementary material related to this article can be found online at https://doi.org/10.1016/j.tca.2024.179883.

Data availability

Data will be made available on request.

References

[1] H. Carslaw, J. Jaeger, Heat Transfer in Solids, Second ed., Oxford University Press, Oxford, 1959.

[2] D.C. Deisenroth, M. Ohadi, Thermal management of high-power density electric motors for electrification of aviation and beyond, Energies 12 (2019) 3594, http://dx.doi.org/10.3390/en12193594.

[3] Y. Lv, G. Zhang, Q. Wang, W. Chu, Thermal management technologies used for high heat flux automobiles and aircraft: A review, Energies 15 (2022) 8316, URL https://www.mdpi.com/1996-1073/15/21/8316.

[4] G. Xia, L. Cao, G. Bi, A review on battery thermal management in electric vehicle application, J. Power Sources 367 (2017) 90–105, http://dx.doi.org/10.1016/j.jpowsour.2017.09.046.

[5] A. Loges, S. Herberger, P. Seegert, T. Wetzel, A study on specific heat capacities of Li-ion cell components and their influence on thermal management, J. Power Sources 336 (2016) 341–350, http://dx.doi.org/10.1016/j.jpowsour.2016.10.049.

[6] H. Zhang, J. Baeyens, G. Cáceres, J. Degreve, Y. Lv, Thermal energy storage: Recent developments and practical aspects, Prog. Energy Combust. Sci. 53 (2016) 1–40, http://dx.doi.org/10.1016/j.pecs.2015.10.003.

[7] S. Hasnain, Review on sustainable thermal energy storage technologies, Part I: heat storage materials and techniques, Energy Convers. Manage. 39 (1998) 1127–1138, http://dx.doi.org/10.1016/S0196-8904(98)00025-9.

[8] J. Lizana, R. Chacartegui, A. Barrios-Padura, J.M. Valverde, Advances in thermal energy storage materials and their applications towards zero energy buildings: A critical review, Appl. Energy 203 (2017) 219–239, http://dx.doi.org/10.1016/j.apenergy.2017.06.008.

[9] P. Shafigh, I. Asadi, N.B. Mahyuddin, Concrete as a thermal mass material for building applications-A review, J. Build. Eng. 19 (2018) 14–25, http://dx.doi.org/10.1016/j.jobe.2018.04.021.

[10] A.M. Khudhair, M. Farid, A review on energy conservation in building applications with thermal storage by latent heat using phase change materials, Energy Convers. Manag. (2021) 162–175, http://dx.doi.org/10.1016/S0196-8904(03)00131-6.

[11] Plastics — Differential scanning calorimetry (DSC) — Part 4: Determination of specific heat capacity, (ISO 11357-4:2021) 2021, URL https://www.iso.org/obp/ui/#iso:std:iso:11357:-4:ed-3:v1:en.

[12] Fine ceramics (advanced ceramics, advanced technical ceramics) — Thermophysical properties of ceramic composites — Determination of specific heat capacity, (ISO 19628:2017) 2017, URL https://www.iso.org/standard/62999.html.

[13] P.K. Gallagher, M.E. Brown, Handbook of Thermal Analysis and Calorimetry, first ed., Elsevier, Amsterdam, 2003.

[14] E.V. Boldyreva, V. Drebushchak, I. Paukov, Y.A. Kovalevskaya, T.N. Drebushchak, DSC and adiabatic calorimetry study of the polymorphs of paracetamol, J. Therm. Anal. Calorim. 77 (2004) 607–623, http://dx.doi.org/10.1023/B:JTAN.0000038998.47606.27.

[15] M. Gustavsson, N. Saxena, E. Karawacki, S. Gustafsson, Specific heat measurements with the hot disk thermal constants analyser, in: Thermal Conductivity 23, CRC Press, 1995, pp. 56–65.

[16] S.A. Al-Ajlan, Measurements of thermal properties of insulation materials by using transient plane source technique, Appl. Therm. Eng. 26 (2006) 2184–2191, http://dx.doi.org/10.1016/j.applthermaleng.2006.04.006.

[17] O. Almanza, M. Rodríguez-Pérez, J. De Saja, Applicability of the transient plane source method to measure the thermal conductivity of low-density polyethylene foams, J. Polym. Sci., Part B: Polym. Phys. 42 (2004) 1226–1234, http://dx.doi.org/10.1002/polb.20005.

[18] T. Log, S. Gustafsson, Transient plane source (TPS) technique for measuring thermal transport properties of building materials, Fire Mater. 19 (1995) 43–49, http://dx.doi.org/10.1002/fam.810190107.

[19] R. Penide-Fernandez, F. Sansoz, Anisotropic thermal conductivity under compression in two-dimensional woven ceramic fibers for flexible thermal protection systems, Int. J. Heat Mass Transfer 145 (2019) 118721, http://dx.doi.org/10.1016/j.ijheatmasstransfer.2019.118721.

[20] H. Zhang, K. Wu, G. Xiao, Y. Du, G. Tang, Experimental study of the anisotropic thermal conductivity of 2D carbon-fiber/epoxy woven composites, Compos. Struct. 267 (2021) 113870, http://dx.doi.org/10.1016/j.compstruct.2021.113870.

[21] P. Ding, J. Zhang, N. Song, S. Tang, Y. Liu, L. Shi, Anisotropic thermal conductive properties of hot-pressed polystyrene/graphene composites in the through-plane and in-plane directions, Compos. Sci. Technol. 109 (2015) 25–31, http://dx.doi.org/10.1016/j.compscitech.2015.01.015.

[22] H. Zheng, K. Jaganandham, Thermal conductivity and interface thermal conductance in composites of titanium with graphene platelets, J. Heat Transfer 136 (2014) 061301, http://dx.doi.org/10.1115/1.4026488.

[23] S. Gustafsson, Transient plane source techniques for thermal conductivity and thermal diffusivity measurements of solid materials, Rev. Sci. Instrum. 62 (1991) 797–804, http://dx.doi.org/10.1063/1.1142087.

[24] Plastics — Determination of thermal conductivity and thermal diffusivity — Part 2: Transient plane heat source (hot disc) method, (ISO 22007-2) 2022, URL https://www.iso.org/standard/81836.html.

[25] D. Hume, A. Sizov, B. Mihiretie, D. Cederkrantz, S.E. Gustafsson, M. Gustavsson, Specific heat measurements of large-size samples with the hot disk thermal constants analyser, in: Thermal Conductivity 33, 2017, p. 10.

[26] N.E. Taylor, D.M. Williamson, Characterising Group Interaction Modelling for Complex Composite Materials, Technical Report, Cavendish Laboratory, University of Cambridge, Cambridge, 2019.

[27] M. Gustavsson, E. Karawacki, S.E. Gustafsson, Thermal conductivity, thermal diffusivity, and specific heat of thin samples from transient measurements with hot disk sensors, Rev. Sci. Instrum. 65 (1994) 3856–3859, http://dx.doi.org/10.1063/1.1145178.

[28] M. Gustavsson, S. Gustafsson, On the use of transient plane source sensors for studying materials with direction dependent properties, in: Thermal Conductivity 26, 2001, p. 367.

[29] S.E. Gustafsson, E. Karawacki, M.A. Chohan, Thermal transport studies of electrically conducting materials using the transient hot-strip technique, J. Phys. D: Appl. Phys. 19 (1986) 727, http://dx.doi.org/10.1088/0022-3727/19/5/007.

[30] Instruction Manual: Hot Disk Thermal Constants Analyser, Hot Disk AB, Sweden, 2022.

[31] B.M. Suleiman, S. Malinarič, Transient techniques for measurements of thermal properties of solids: data evaluation within optimized time intervals, WSEAS Trans. Heat Mass Transf. 1 (2006).

[32] E. Karawacki, B.M. Suleiman, Dynamic plane source technique for simultaneous determination of specific heat, thermal conductivity and thermal diffusivity of metallic samples, Meas. Sci. Technol. 2 (1991) 744, http://dx.doi.org/10.1088/0957-0233/2/8/007.

[33] S. Tarasovs, A. Aniskevich, Identification of the anisotropic thermal conductivity by an inverse solution using the transient plane source method, Measurement 206 (2023) 112252, http://dx.doi.org/10.1016/j.measurement.2022.112252.

[34] A. Elkholy, H. Sadek, R. Kempers, An improved transient plane source technique and methodology for measuring the thermal properties of anisotropic materials, Int. J. Therm. Sci. 135 (2019) 362–374, http://dx.doi.org/10.1016/j.ijthermalsci.2018.09.021.

[35] H. Zhang, Y. Li, W. Tao, Theoretical accuracy of anisotropic thermal conductivity determined by transient plane source method, Int. J. Heat Mass Transfer 108 (2017) 1634–1644, http://dx.doi.org/10.1016/j.ijheatmasstransfer.2017.01.025.

[36] R. Coquard, E. Coment, G. Flasquin, D. Baillis, Analysis of the hot-disk technique applied to low-density insulating materials, Int. J. Therm. Sci. 65 (2013) 242–253, http://dx.doi.org/10.1016/j.ijthermalsci.2012.10.008.

[37] Q. Zheng, S. Kaur, C. Dames, R.S. Prasher, Analysis and improvement of the hot disk transient plane source method for low thermal conductivity materials, Int. J. Heat Mass Transfer 151 (2020) 119331, http://dx.doi.org/10.1016/j.ijheatmasstransfer.2020.119331.

[38] S. Wang, Q. Ai, T. Zou, C. Sun, M. Xie, Analysis of radiation effect on thermal conductivity measurement of semi-transparent materials based on transient plane source method, Appl. Therm. Eng. 177 (2020) 115457, http://dx.doi.org/10.1016/j.applthermaleng.2020.115457.

[39] H. Zhang, Y. Li, W. Tao, Effect of radiative heat transfer on determining thermal conductivity of semi-transparent materials using transient plane source method, Appl. Therm. Eng. 114 (2017) 337–345, http://dx.doi.org/10.1016/j.applthermaleng.2016.11.208.

[40] H. Zhang, M. Li, W. Fang, D. Dan, Z. Li, W. Tao, A numerical study on the theoretical accuracy of film thermal conductivity using transient plane source method, Appl. Therm. Eng. 72 (2014) 62–69, http://dx.doi.org/10.1016/j.applthermaleng.2014.01.058.

[41] A. Berge, B. Adl-Zarrabi, C.-E. Hagentoft, Determination of specific heat capacity by transient plane source, Front. Archit. Res. 2 (2013) 476–482, http://dx.doi.org/10.1016/j.foar.2013.09.004.

[42] J. Yves, A. Zoubir, A quadrupolar complete model of the hot disc, Meas. Sci. Technol. 18 (2007) 1229, http://dx.doi.org/10.1088/0957-0233/18/5/009.

[43] V. Bohac, M.K. Gustavsson, L. Kubicar, S.E. Gustafsson, Parameter estimations for measurements of thermal transport properties with the hot disk thermal constants analyzer, Rev. Sci. Instrum. 71 (2000) 2452–2455, http://dx.doi.org/10.1063/1.1150635.

[44] J.-G. Bauzin, N. Laraqi, New thermal analysis of the hot disc method based on explicit analytical developments, Int. J. Therm. Sci. 195 (2024) 108645, http://dx.doi.org/10.1016/j.ijthermalsci.2023.108645.

[45] V. Mathur, K. Sharma, Thermal response of polystyrene/poly methyl methacrylate (PS/PMMA) polymeric blends, Heat Mass Transf. 52 (2016) 2901–2911, http://dx.doi.org/10.1007/s00231-016-1779-4.

[46] Z. Zeng, W. Dilles, B.M. Mihiretie, Enhancing thermal characterization with TPS method: a study of specific heat capacity and anisotropic heat flow using FEM, in: Proceedings of the 17th International Heat Transfer Conference, 2023, p. 1141.

[47] A.C. Lua, J. Su, Isothermal and non-isothermal pyrolysis kinetics of Kapton® polyimide, Polym. Degrad. Stab. 91 (2006) 144–153, http://dx.doi.org/10.1016/j.polymdegradstab.2005.04.021.

[48] J.V. Beck, K.J. Arnold, Parameter Estimation in Engineering and Science, first ed., Wiley, 1977.

[49] K.J. Dowding, B.F. Blackwell, R.J. Cochran, Application of sensitivity coefficients for heat conduction problems, Numer. Heat Transf. B: Fundam. 36 (1999) 33–55, http://dx.doi.org/10.1080/104077999275767.

[50] N.P. Ramos, L.F. dos Santos Carollo, et al., Contact resistance analysis applied to simultaneous estimation of thermal properties of metals, Meas. Sci. Technol. 31 (2020) 105601, DOI: 10.0.4.64/1361-6501/ab8e6a.
[51] G. D'Alessandro, F. de Monte, On the optimum experiment and heating times when estimating thermal properties through the plane source method, Heat Transf. Eng. 43 (2021) 257–269, http://dx.doi.org/10.1080/01457632.2021.1874655.
[52] M.J. Powell, et al., The BOBYQA Algorithm for Bound Constrained Optimization Without Derivatives, Cambridge NA Report NA2009/06, vol. 26, University of Cambridge, Cambridge, 2009, pp. 26–46.
[53] H. Zhang, C. Shang, G. Tang, Measurement and identification of temperature-dependent thermal conductivity for thermal insulation materials under large temperature difference, Int. J. Therm. Sci. 171 (2022) 107261, http://dx.doi.org/10.1016/j.ijthermalsci.2021.107261.
[54] P.R. Bevington, D.K. Robinson, Data Reduction and Error Analysis, third ed., McGraw Hill Higher Education, New York, 2003.